doi:10.3788/gzxb20144303.0313001

低串扰聚合物交叉耦合串联五环谐振电光开关

郑传涛[1],罗倩倩[1],孙长轮[1,2],杜巧玲[1],张大明[1],王一丁[1]
(1 吉林大学 电子科学与工程学院 集成光电子学国家重点联合实验室吉林大学实验区,长春 130012)
(2 吉林大学 物理学院,长春 130012)

摘 要:利用两组串联五环谐振器以及它们与两信道波导的交叉耦合作用,优化设计并模拟了一种超低串扰 2×2 新型聚合物电光开关.为了表征器件的输出光功率特性,给出了器件结构、分析理论和相关公式.为了在下行端口(drop 端口)得到箱型光谱响应以及极低的串扰和插入损耗,优化了微环谐振级数和耦合间距.对器件输出光功率和输出光谱的模拟分析结果显示,器件交叉和直通态间的切换电压为 4 V,交叉和直通态下两端口间的串扰分别为 −66 dB 和 −54.7 dB,插入损耗分别为 2.34 dB 和 0.24 dB.在 1 GHz 方波信号作用下,器件 drop 端口的上升和下降时间分别为 15 ps 和 90 ps.由于聚合物微环的弯曲半径仅为 19.45 μm,因此该器件具有超紧凑的尺寸,其长度和宽度仅为 0.407 mm,约为马赫-曾德尔干涉仪或者定向耦合器等一般结构聚合物电光开关长度的 1/10.依赖于小的封装尺寸和极低的串扰,该器件可以高密度地集成在光电子芯片上,在光片上网络中光信号的控制方面具有潜在的应用.

关键词:集成光电子;光波导器件;电光开关;微环谐振器;聚合物
中图分类号:TN253 **文献标识码**:A **文章编号**:1004-4213(2014)03-0313001-7

Polymer Electro-optic Switch Using Cross-coupling Five-serial-coupled Microring Resonator with Ultra-low Crosstalk

ZHENG Chuan-Tao[1], LUO Qian-Qian[1], SUN Chang-Lun[1,2],
DU Qiao-Ling[1], ZHANG Da-Ming[1], WANG Yi-Ding[1]
(1 *State Key Laboratory on Integrated Optoelectronics, College of Electronic Science and Engineering, Jilin University, Changchun* 130012, *China*)
(2 *College of Physics, Jilin University, Changchun* 130012, *China*)

Abstract: A novel 2×2 polymer electro-optic switch was optimized and simulated based on two-group five-serial-coupled microring resonator and their cross-coupling with two channel waveguides. Detailed structure, theory and formulation were available to characterize the output powers of the switch. For realizing boxlike spectrum (drop port) as well as low crosstalk and insertion loss, resonance order and coupling gaps were optimized. Analysis and simulation on output powers and output spectrum indicated that, a switching voltage of about 4.0 V was desired to realize the exchange between cross-state and bar-state; the crosstalk under cross state and bar state were extremely low as −66 dB and −54.7 dB, respectively; the insertion losses under the two operation states were 2.34 dB and 0.24 dB, respectively. For the drop port, the 10%～90% rise time and fall time were estimated to be 15 ps and 90 ps, respectively, under the operation of 1 GHz switching operation. The bending radius of each electro-optic polymer microring was as small as 19.45 μm, leading to ultra-compact size of only 0.407 mm in both length and width, which was nearly 1/10 of the length of Mach-Zehnder interferometer or directional coupler type polymer electro-optic switches. Consequently, because of small footprint size and extremely

Foundation item: The National Natural Science Foundation Council of China (Nos. 61107021, 61177027, 61077041 and 61001006), the Ministry of Education of China (Nos. 20110061120052 and 20120061130008), the China Postdoctoral Science Foundation funded project (Nos. 20110491299, 2012T50297), the Science and Technology Department of Jilin Province of China (No. 20130522161JH), and the Special Funds of Basic Science and Technology of Jilin University (Nos. 201103076, 200905005)
First author: ZHENG Chuan-Tao (1982-), male, Associate Professor, Ph. D. degree, mainly focuses on guided-wave optics and optoelectronics. Email: zhengchuantao@jlu.edu.cn
Received: Jul. 10, 2013; **Accepted**: Aug. 14, 2013

low crosstalk, this switching configuration can be densely integrated onto optoelectronic chips, and thus it possesses potential applications in optical signal control in optical networks-on-chip.

Key words: Integratd optoelectronics; Waveguide device; Electro-optic switch; Microring resonator; Polymer

OCIS Codes: 130.0250;130.2790;230.2090

0 Introduction

Electro-optic (EO) switches[1-2] are important components in optical communication systems, optical sensing systems, *etc*. Poled polymer materials[3-4] are widely used in the fabrication of EO switches and modulators. Within the available optical switches, micro-ring resonator (MRR)-based optical switches are typically preferred due to their ultra-compact size, simple-mode resonances, and ease of phase-matching between an MRR and its coupling waveguides. Besides, the MRR structure is more convenient for building large switching arrays by cascading fundamental element. Until now, the reported MRR EO switches either in experiment or in theory are generally the carrier-injection based silicon or GaAs ones, for example, the single-ring based silicon MRR switch [5], the double-ring based silicon MRR switch [6] and GaAs MRR switch [7], the ten-ring coupled silicon MRR switch [8], and the interferometry silicon MRR switch [9].

Different from the silicon or GaAs MRR switches, this paper aimed at providing a novel 2×2 switching scheme based on poled polymer materials. The main achievements of this paper were described below. First, small footprint device based on microring resonator (MRR) structure. Air was used as left/right cladding, which created high index contrast between core index and left/right cladding index for the ring waveguide and leaded to an ultra-small bending radius. Second, By using two-group five-serial-coupled microrings (ten rings) which were cross-coupled with one parallel channel waveguide and one vertical channel waveguide, a novel 2×2 switching configuration was proposed, which revealed boxlike flat spectral response, small device size and ultra-low crosstalk of less than −50 dB under both operation states, compared with the simple single-ring coupled MRR switch [10] and our previously reported directional coupler (DC) EO switches [11-12] or Mach-Zehnder interferometer (MZI) switch [13].

1 Structure and Theory

1.1 Device structure and basic parameters

The structure model of the cross/bar polymer EO routing switch has been shown in Fig. 1. The device consists of a horizontal channel, a vertical channel and two-group five-serial-coupled microrings with identical ring radius. The waveguide cross-section over the coupling plane between two adjacent microrings has been shown in Fig. 2. For the MRR waveguide, the layers are as: upper confined layer, upper electrode, upper buffer layer, EO core, under buffer layer, under electrode, Si substrate. The electrodes are only deposited on microrings, so the EO effect only occurs in the waveguide cores of all microrings. By applying different operation voltages on microrings, the switching functions can be realized between the horizontal channel and the vertical channel.

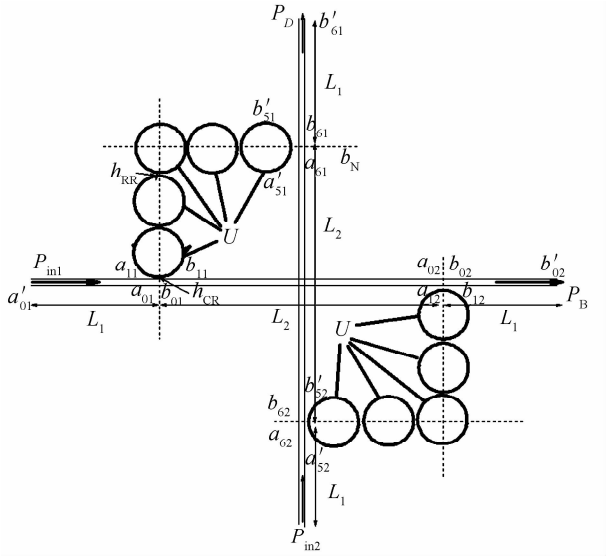

Fig. 1 Structure model of the cross/bar polymer MRR EO switch

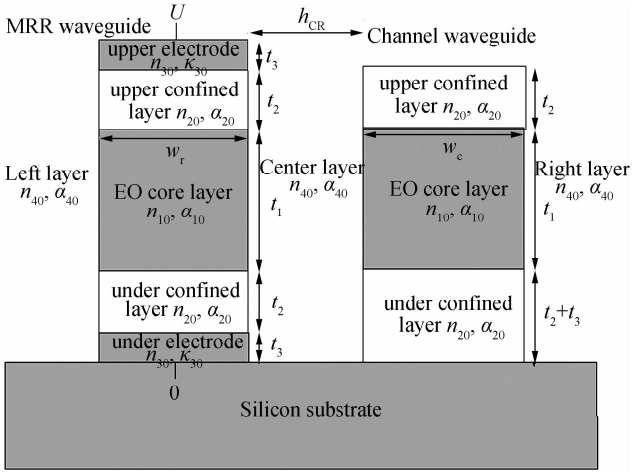

Fig. 2 Waveguide cross-section between MRR waveguide and channel waveguide

Under the resonance wavelength of 1 550 nm, relative material parameters are taken as: the refractive

index of the EO polymer material (AJL8/APC) $n_{10}=1.59$, its bulk amplitude attenuation coefficient $\alpha_{10}=0.25$ dB/cm, and its EO coefficient $\gamma_{33}=68$ pm/V[14]; the refractive index of the upper/under buffer layer material [poly (pentafluorostyrene-co-glycidyl methacrylate), P(PFS-GMA)] $n_{20}=1.461$, and its bulk amplitude attenuation coefficient $\alpha_{20}=0.25$ dB/cm[15]; the electrode is made of aurum, its refractive index $n_{30}=0.19$, and its bulk extinction coefficient $\kappa_{30}=6.1$[16]. Besides, the input waveguide length is designed to be $L_1=100$ μm. Air, with an index of only 1.0 as well as no absorption loss, is adopted as the left/right cladding layer, e.g. $n_{40}=1.0$ and $\alpha_{40}=0$.

The upper/under buffer layer thickness is taken as $t_2=2.5$ μm, and the electrode thickness is taken as $t_3=0.2$ μm. For assuring single-mode propagation in microring rectangular waveguide, its width and thickness are both taken as $w_r=t_1=1.7$ μm. We take the ring bending radius as $R=19.49$ μm, and the calculated mode effective refractive index is about 1.5189, under the case of applying no voltage. We take the core thickness of the channel equals that of the microring as $t_1=1.7$ μm and select the width of the channel waveguide as $w_c=1.85$ μm, and in this case, the channel and microring possess identical mode effective refractive index. Besides, under the above parameters, the mode loss in MRR waveguide is almost equal to that of the channel waveguide, which are $\alpha_R=\alpha_C=0.256$ dB/cm. The coupling gap between two adjacent microrings and that between the microring waveguide and channel waveguide are h_{RR} and h_{CR}, respectively, the resonance order of microring is denoted by m, and these three parameters will be optimized in Section 2.

With poling on the polymer along the vertical direction, the obtained EO coefficient γ_{33} is the largest one within all 18 elements[17]. To make best use of this element, the applied voltage should be along the vertical direction (y-direction), and also the electric component of the optical field should also be along the y-direction. Then, the selected mode should be E_{mn}^{y}, whose mode components are H_x and E_y. Therefore, the device reveals obvious polarization characteristics, since it does not work for E_{mn}^{x} mode with E_x component.

1.2 Theory and formulation

Analysis of the five-serial-coupled microrings is divided into three sections, including the transfer matrix of the first two microings (defined as $\boldsymbol{P}_{2R}$), that of the center microring (defined as $\boldsymbol{M}$), and that of the second two microrings (defined as $\boldsymbol{P}_{2R}$). They are obtained by using the transfer matrix method as follows

$$\boldsymbol{P}_{2R}=\frac{1}{j\kappa_{RR}}\begin{bmatrix}0 & \exp(-j\varphi_{R1})\\ \exp(j\varphi_{R1}) & 0\end{bmatrix}\times\begin{bmatrix}-\exp(j\varphi_{R1}) & t_{RR}\exp(-j\varphi_{R1})\\ -t_{RR}\exp(j\varphi_{R1}) & \exp(-j\varphi_{R1})\end{bmatrix} \tag{1}$$

$$\boldsymbol{M}=\frac{1}{j\kappa_{RR}}\begin{bmatrix}t_{RR} & -1\\ 1 & -t_{RR}\end{bmatrix}\begin{bmatrix}0 & \exp(-j\varphi_{R2})\\ \exp(j\varphi_{R3}) & 0\end{bmatrix}\times\frac{1}{j\kappa_{RR}}\begin{bmatrix}t_{RR} & -1\\ 1 & -t_{RR}\end{bmatrix} \tag{2}$$

where $\varphi_{R1}=\pi R(\beta_R-j\alpha_R)$, $\varphi_{R2}=0.5\pi R(\beta_R-j\alpha_R)$, $\varphi_{R3}=1.5\pi R(\beta_R-j\alpha_R)$, and κ_{RR} and t_{RR} are the amplitude coupling ratio and amplitude transmission ratio between two adjacent microrings, respectively. Finally, the transfer matrix of the five-serial-coupled microrings is obtained by using the transfer matrix method as

$$\boldsymbol{M}_t=\boldsymbol{P}_{2R}\boldsymbol{M}\boldsymbol{P}_{2R} \tag{3}$$

According to EO modulation theory, we can obtain the variation of the refractive index Δn_{10} of the core EO material versus the operation voltage U as

$$\Delta n_{10}(U)=\frac{1}{2}n_{10}^3\gamma_{33}E_1=\frac{n_{10}^3n_{20}^2\gamma_{33}U}{2(2n_{10}^2t_2+n_{20}^2t_1)} \tag{4}$$

where U can be equal to zero or not. The refractive index of the core EO material of the microring n_{10} will be changed to $n_{10}+\Delta n_{10}$. Then the mode propagation constant in each microring can be regarded as a function of U, denoted by $\beta_R(U)$. Note that $\boldsymbol{M}_t$ is a function of U, that is, $\boldsymbol{M}_t=\boldsymbol{M}_t(U)$.

The case of the light inputting into the horizon waveguide only and that of the light inputting into the vertical waveguide only can be similarly analyzed, and the first case is only considered here. In the following analysis, the resonance of the two-group MRRs with the two channel waveguides are both considered. Let a_{01} be the input light amplitude into the left coupling point of the horizontal channel, b_{61} be the output light amplitude from the upper coupling point of the vertical channel, and b_{02} be the output light amplitude from the right coupling point of the horizontal channel. Define κ_{CR} and t_{CR} as the amplitude coupling ratio and amplitude transmission ratio between channel and microring, respectively, and they satisfy the relation of $\kappa_{CR}^2+t_{CR}^2=1$. By using CMT, we obtain the following relations

$$b_{01}=t_{CR}a_{01}-j\kappa_{CR}a_{11} \tag{5}$$
$$b_{11}=t_{CR}a_{11}-j\kappa_{CR}a_{01} \tag{6}$$
$$b_{61}=t_{CR}a_{61}-j\kappa_{CR}a_{51}' \tag{7}$$
$$b_{51}'=t_{CR}a_{51}'-j\kappa_{CR}a_{51} \tag{8}$$
$$b_{02}=t_{CR}a_{02}-j\kappa_{CR}a_{12} \tag{9}$$
$$b_{12}=t_{CR}a_{02}-j\kappa_{CR}a_{02} \tag{10}$$
$$b_{52}'=t_{CR}a_{52}' \tag{11}$$
$$b_{52}'=-j\kappa_{CR}a_{52}' \tag{12}$$

The relation between a_{02} and b_{01} and that between a_{61}

and b_{62} are

$$a_{61}=b_{62}\exp(-\mathrm{j}\psi_2) \tag{13}$$

$$a_{02}=b_{01}\exp(-\mathrm{j}\psi_2) \tag{14}$$

where $\psi_2=L_2(\beta_C-\mathrm{j}\alpha_C)$. By using Eq. (3), we derived

$$\begin{bmatrix}a'_{51}\\b'_{51}\end{bmatrix}=\begin{bmatrix}\boldsymbol{M}_t(1,1) & \boldsymbol{M}_t(1,2)\\ \boldsymbol{M}_t(2,1) & \boldsymbol{M}_t(2,2)\end{bmatrix}\begin{bmatrix}a_{11}\\b_{11}\end{bmatrix} \tag{15}$$

$$\begin{bmatrix}a'_{52}\\b'_{52}\end{bmatrix}=\begin{bmatrix}\boldsymbol{M}_t(1,1) & \boldsymbol{M}_t(1,2)\\ \boldsymbol{M}_t(2,1) & \boldsymbol{M}_t(2,2)\end{bmatrix}\begin{bmatrix}a_{12}\\b_{12}\end{bmatrix} \tag{16}$$

Combining Eqs. (5)～(16), we obtain the output powers from the drop port and through port as, respectively

$$P_B(\mathrm{dB})=10\lg\left|\frac{b_{02}}{a_{01}}\exp(-\mathrm{j}2\psi_1)\right|^2=10\lg\left|\frac{f_3f_5}{f_6}\exp(-\mathrm{j}2\psi_1)\right|^2 \tag{17}$$

$$P_D(\mathrm{dB})=10\lg\left|\frac{b_{2N+2,1}}{a_{01}}\exp(-\mathrm{j}2\psi_1)\right|^2=10\lg|f_7\exp(-\mathrm{j}2\psi_1)|^2 \tag{18}$$

where β_C and α_C are the mode propagation constant and mode loss coefficient of the channel waveguide, respectively, $\psi_1=L_1(\beta_C-\mathrm{j}\alpha_C)$, and with the definition of $\boldsymbol{M}_t^{-1}$ as the invert matrix of $\boldsymbol{M}_t$, other parameters are listed below

$$f_1=\frac{[\boldsymbol{M}_t^{-1}(1,1)+\boldsymbol{M}_t^{-1}(1,2)t_{CR}]\boldsymbol{M}_t(1,2)}{1-[\boldsymbol{M}_t^{-1}(1,1)+\boldsymbol{M}_t^{-1}(1,2)t_{CR}]\boldsymbol{M}_t(1,1)} \tag{19a}$$

$$f_2=\frac{-\mathrm{j}\kappa_{CR}\exp(-\mathrm{j}\psi_2)}{1-t_{CR}f_1} \tag{19b}$$

$$f_3=t_{CR}\exp(-\mathrm{j}\psi_2)-\mathrm{j}\kappa_{CR}f_1f_2 \tag{19c}$$

$$f_4=-\mathrm{j}\kappa_{CR}\exp(-\mathrm{j}\psi_2)\cdot[\boldsymbol{M}_t(1,1)f_1+\boldsymbol{M}_t(1,2)]f_2 \tag{19d}$$

$$f_5=t_{CR}-\kappa_{CR}^2\boldsymbol{M}_t(1,2)[\boldsymbol{M}_t^{-1}(1,1)+\boldsymbol{M}_t^{-1}(1,2)t_{CR}]-t_{CR}[\boldsymbol{M}_t^{-1}(1,1)+\boldsymbol{M}_t^{-1}(1,2)t_{CR}][\boldsymbol{M}_t(1,1)+\boldsymbol{M}_t(1,2)t_{CR}] \tag{19e}$$

$$f_6=1+\kappa_{CR}^2\boldsymbol{M}_t^{-1}(1,2)f_4-[\boldsymbol{M}_t^{-1}(1,1)+\boldsymbol{M}_t^{-1}(1,2)t_{CR}]\times[\boldsymbol{M}_t(1,1)+\boldsymbol{M}_t(1,2)t_{CR}] \tag{19f}$$

$$f_7=\frac{f_5}{f_6}[t_{CR}f_4+\boldsymbol{M}_t(1,1)+\boldsymbol{M}_t(1,2)t_{CR}]-\{t_{CR}[\boldsymbol{M}_t(1,1)+\boldsymbol{M}_t(1,2)t_{CR}]+\kappa_{CR}^2\boldsymbol{M}_t(1,2)\} \tag{19g}$$

2 Parameter optimization

The aim of parameter optimization is to make the crosstalk and insertion loss as low as possible under $U=0$ V (drop state). Based on the resonance theory on serial-coupled microrings [17], the resonance order (m) and two coupling gaps (h_{RR} and h_{CR}) will influence the shape and flatness of output spectrum and then affect the crosstalk and insertion loss. Therefore, they should all be optimized.

2.1 Optimization on resonance order m

Under $U=0$ V, the switch is operated at cross state. By using Eqs. (17) and (18), we first analyzed the effect of resonance order on the output powers of the switch, as shown in Fig. 3(a), where the resonance order is taken as $m=60$, 80, 120 and 160, and the two coupling gaps are $h_{RR}=0.68$ μm and $h_{CR}=0.14$ μm. It can be found that when m is too small, e.g. $m=60$, the output power from the horizon channel is larger than that from the vertical channel, and the cross state cannot be realized. So m shouldn't be taken too small. When m increases to 80, the resonance light power from the horizon channel drops to (40 dB, but the spectrum is not flat over the wavelength range around 1 550 nm. An extremely low crosstalk (P_B-P_D) can be achieved as m increases to 120; however, as m is equal to 160, the crosstalk increases. The curves of insertion loss and crosstalk under cross state versus m are shown in Fig. 3(b). One can find that the values of m are different for the two cases to obtain the minimum crosstalk, but they almost reach to their smallest values under $m=120$. Therefore, m is taken as 120.

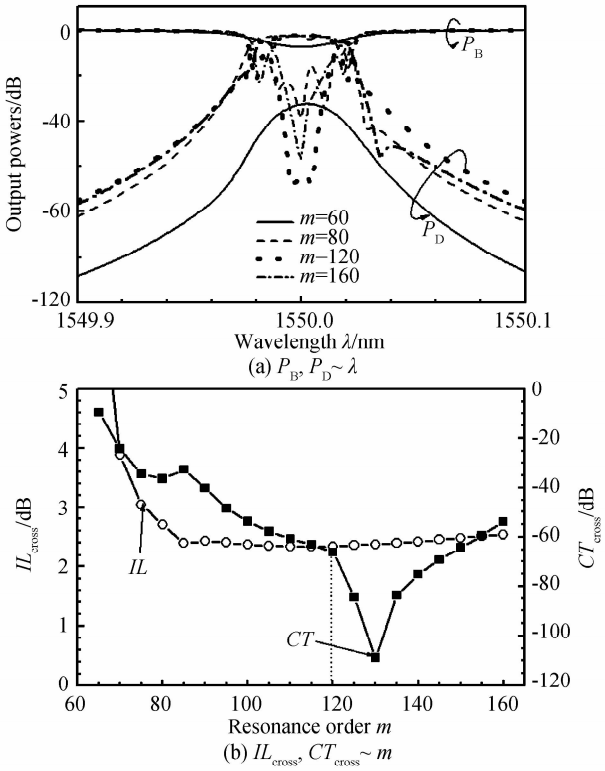

Fig. 3 Effects of resonance order m on the output powers, curves of insertion loss and crosstalk under cross state

2.2 Optimization on coupling gap h_{RR}

The effects of the coupling gap h_{RR} on the output powers P_B and P_D are shown in Figs. 4(a) and 4(b), respectively, where $h_{CR}=0.14$ μm, $h_{RR}=0.48$, 0.68, 0.88 and 1.08 μm. One can find that when h_{RR} is too small, the output power from the through port reveals extremely large vibration; while when h_{RR} is too large, the device cannot realize cross state. The influences of h_{RR} on insertion loss and crosstalk are further illustrated in Fig. 4(c). We observe that h_{RR} should be selected as small as possible to decrease

insertion loss, and when $h_{RR} = 0.68\mu m$, the crosstalk reaches to its minimum value. So we selected $h_{RR} = 0.68\ \mu m$.

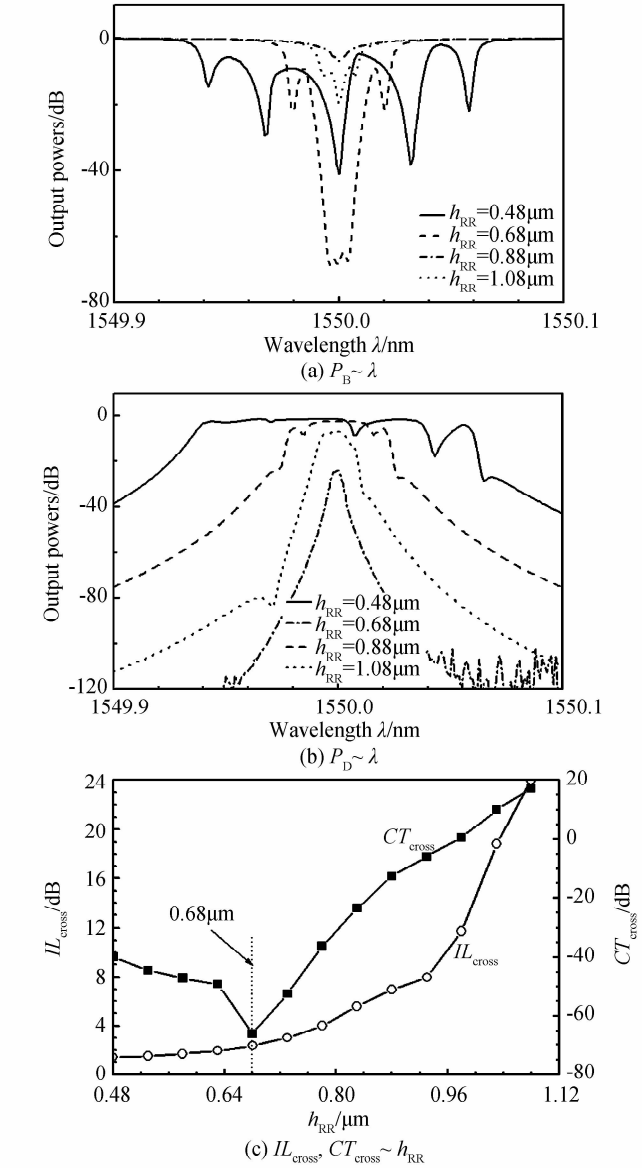

Fig. 4 Effects of coupling gap h_{RR} on the output powers, curves of insertion loss and crosstalk under cross state

2.3 Optimization on coupling gap h_{CR}

The effects of the coupling gap h_{CR} on the output powers P_B and P_D are shown in Figs. 5(a) and 5(b), respectively, where $h_{RR} = 0.68\ \mu m$, $h_{CR} = 0.08$, 0.14, 0.20, 0.26 μm. We can see that when h_{CR} is too small or too large, the output power from the drop port reveals extremely large vibration, and the crosstalk under this state does not reach to the minimum value. The influences of h_{CR} on insertion loss and crosstalk are detailed illustrated in Fig. 5(c). It can be determined that when $h_{CR} = 0.14\ \mu m$, both insertion loss and crosstalk reach to their minimum values. So we select $h_{CR} = 0.14\ \mu m$.

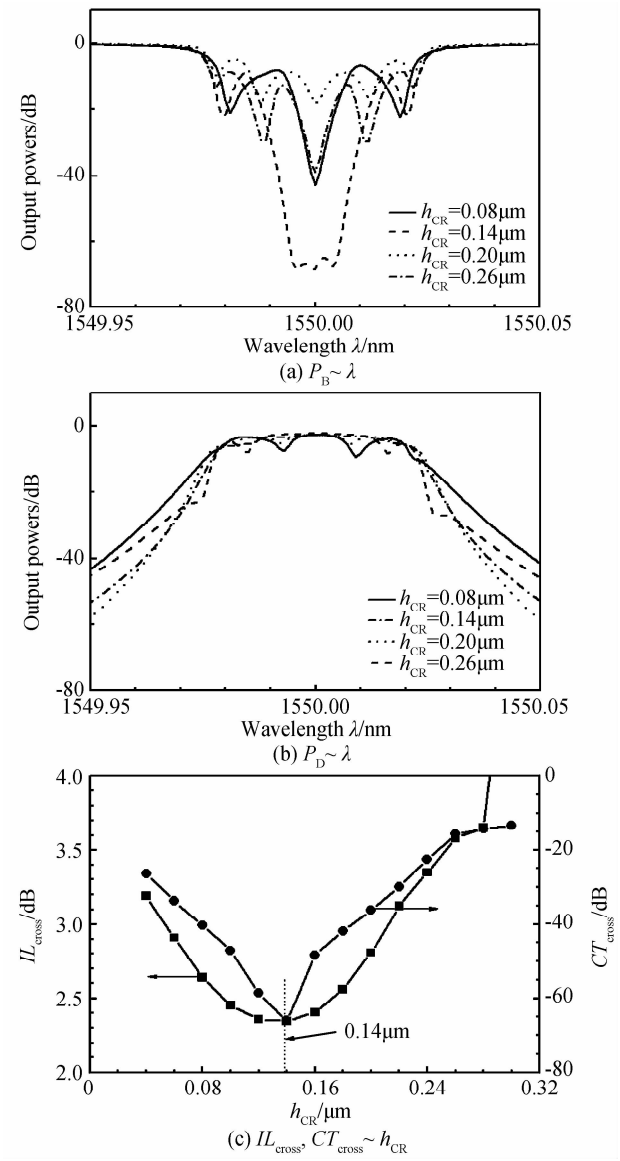

Fig. 5 Effects of the coupling gap h_{CR} on the output powers, curves of insertion loss and crosstalk under cross state

3 Characteristics analysis

3.1 Output powers versus applied voltage

After optimization, we investigated the switching and spectral characteristics of the device. By using Eqs. (17) and (18), Fig. 6 presents the curves of output powers P_B and P_D from the drop and through ports versus the applied voltage U under 1 550 nm wavelength. One can observe that when $U \leqslant 0.01$ V, P_D is the maximum, and the switch is operated at cross state; as U increases, P_B gets larger and P_D gets smaller, and the larger U is, the smaller P_D becomes and the lower the crosstalk ($P_D - P_B$) becomes. As a comparison, the output powers versus applied voltage of the device with three rings in a group are also plotted in Fig. 5. They show the same trend as those of the device with five rings.

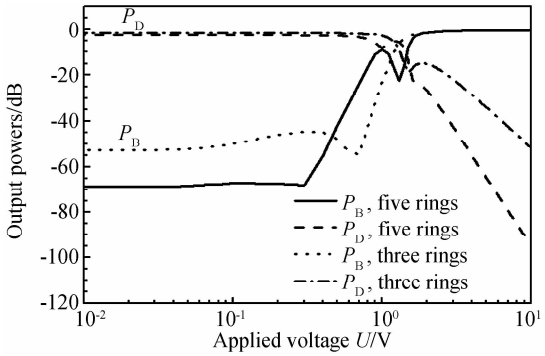

Fig. 6 Curves of output powers P_B and P_D from the drop and through ports versus the applied voltage U

3.2 Crosstalk and switching voltage

The relations between the device′s crosstalk (CT_{bar} and CT_{cross}) and the difference value of P_D-P_B can be described as

$$-CT_{cross}=P_D-P_B, P_D>P_B \quad (20)$$

$$CT_{bar}=P_D-P_B, P_B>P_D \quad (21)$$

Fig. 7 presents the curves of the difference value P_D-P_B versus the applied voltage U. In this figure, when $P_D-P_B>0$, the switch is under cross state, and the value represents $-CT_{cross}$, as marked in the figure; when $P_D-P_B<0$, the switch is under bar state, and the value represents CT_{bar}, as also marked in the figure. One can observe that as $U\leqslant 0.01$ V, the values of CT_{cross} is as low as -66 dB. A larger U will be helpful for decreasing the crosstalk under bar state, and for obtaining the same wavelength turning range, the applied voltage (e. g. switching voltages) of the switch is taken as $U_s=4$ V. Under this case, the crosstalk under bar state is -54.7 dB. The two crosstalks are obviously lower than those of the device with three rings, which are -51.2 and -28.8 dB under cross state and bar state, respectively.

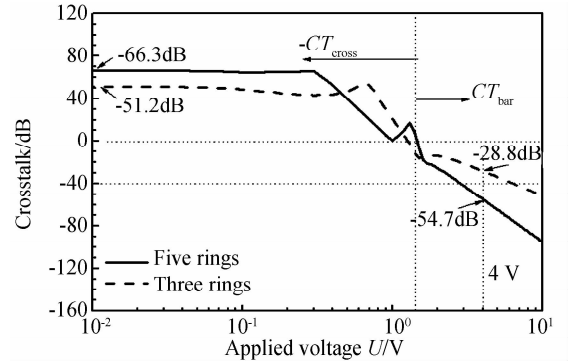

Fig. 7 Curve of the difference value P_D-P_B versus the applied voltage U

3.3 Output spectrum

Under the operations of two state driving voltages ($U=0$ V for cross state and $U=4$ V for bar state), Fig. 8 shows the spectral response of the switch under both operation states. The simulation results indicate that, under the applied voltages of 0 and 4 V, the switch performs good switching functions at 1550 nm wavelength, and it reveals boxlike spectral responses for the drop port as well as extremely low crosstalk for both states. The insertion loss at bar state is about 0.24 dB, while that is about 2.34 dB under cross state. The crosstalk at bar state is -54.7 dB, while that at cross state is about -66 dB.

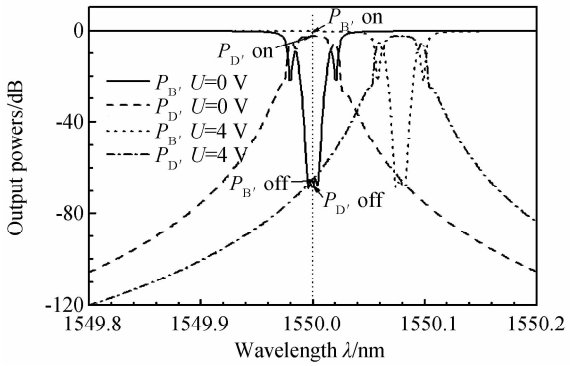

Fig. 8 Spectral response of the MRR switch under both operation states

3.4 Estimation on response time

Since the cross/bar switch is driven in lumped manner, under the operation of a square-wave voltage, the electrical response on the electrode can be calculated by

$$u_e(t)=F^{-1}[V_g(\omega)H(\omega)] \quad (22)$$

where $V_g(\omega)$ is the Fourier transformation of the applied voltage, and $H(\omega)$ is the transfer function of the device. By using Eq. (22) as well as Eqs. (17) and (18), the dynamic response of the switch under the operation of 1GHz square-wave signal (4-V_{pp}, 2-V_{bias}, 1 GHz) is shown in Fig. 9. For the drop port, the 10～90% rise time and fall time are estimated to be $t_r=15$ ps and $t_f=90$ ps, respectively.

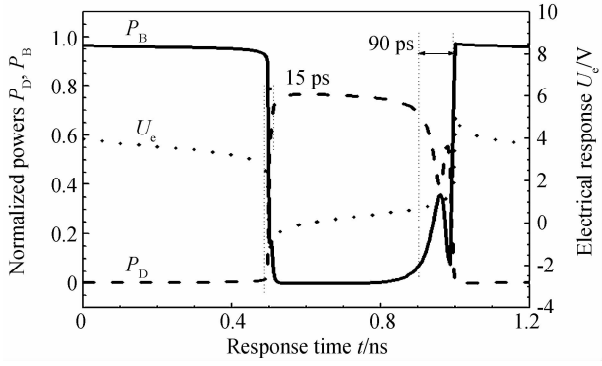

Fig. 9 Dynamic responses under 1 GHz switching operation

3.5 Comparison and discussion

As shown in Table 1, we made a comparison on the performances of this 2×2 cross/bar MRR switch and those of our previously reported 2×2 or 1×2 EO switches based on DC, Y-fed DC, MZI and multimode interference (MMI) MZI structures. It can be found that, the total length of this device is only 0.407 mm, which is much shorter than that of other four devices

(3.1 mm at least for a 1×2 device, and 4.1 mm at least for a 2×2 device), and this device reveals low insertion loss extremely at bar state (about 0.24 dB). This device also has extremely low crosstalk as when compared with other non-resonance switches, which are as low as −54.7 dB and −66 dB under bar and cross states, respectively. Furthermore, this switching scheme shows lower crosstalk than the MRR EO switch (<−20 dB) with only one microring coupled with two parallel waveguides.

Table 1 Comparisons among this MRR switch and our previously reported four polymer EO switches

Structure	U_s/V	IL_{bar}, IL_{cross}/dB	CT_{bar} CT_{cross}/dB	L_{total}/mm
DC 2×2[11]	1.64	1.98 1.98	<−30 <−30	4.139
Y-fed Coupler 1×2[12]	1.78	1.42 1.42	<−30 <−30	3.126
MZI 2×2[13]	2.23	2.64 2.64	<−30 <−30	5.049
MMI-MZI 2×2[18]	1.37	3.75 3.75	<−42 <−42	5.000
MRR 1×2[10]	10.0	0.35 1.20	<−20 <−20	4.000
MRR 2×2 (this)	4.00	0.24 2.34	<−54 <−66	0.407

4 Conclusions

A cross/bar EO routing switch using two-group five-serial-coupled microrings was optimized. Simulation results show that the device possesses boxlike flat spectral response (drop port) by using two-group cross-coupling five-serial-coupled microrings. The switching voltage is about 4.0 V, the crosstalks under cross state and bar state are extremely low as −66 dB and −54.7 dB, respectively, and the insertion losses under cross state and bar state are 2.34 dB and 0.24 dB, respectively. Another superiority of this device is its ultra-compact size of only 0.407 mm in both length and width, which is nearly 1/10 of the length of MZI or DC type polymer EO switches.

References

[1] CHEN C, ZHANG F, WANG H, *et al*. UV curable electro-optic polymer switch based on direct photo definition technique [J]. *IEEE Journal of Quantum Electronics*, 2011, **47**(7): 959-964.

[2] YAN A M, ZHI Y N, SUN J F, *et al*. Design and experiment of a large aperture digital beam deflector based on electro-optic crystal switch array [J]. *Applied Physics B: Lasers and Optics*, 2012, **107**(2): 421-427.

[3] TSUBOI Y, TSUBOI K, MICHINOBU T. Simultaneous formation of donor-acceptor chromophores and cross-linking for electro-optic polymer materials [J]. *Journal of Photopolymer Science and Technology*, 2011, **24**(3): 305-309.

[4] CABANETOS C, BLART E, PELLEGRIN Y, *et al*. Simpler and more efficient strategy to stabilize the chromophore orientation in electro-optic polymers with copper-free thermal Huisgen reaction[J]. *Polymer*, 2011, **52**(10): 2286-2294.

[5] TAKAHASHI K, KANAMORI Y, KOKUBUN Y, *et al*. A wavelength-selective add-drop switch using silicon microring resonator with a submicron-comb electronicstatic actuator[J]. *Optics Express*, 2008, **16**(19): 14421-14428.

[6] SIMOS H, BOGRIS A, RAPTIS N, *et al*. Dynamic properties of a WDM switching module based on active microring resonators[J]. *IEEE Photonic Technology Letters*, 2010, **22**(4): 206-208.

[7] RAVINDRAN S, DATTA A, ALAMEH K, *et al*. GaAs based long-wavelength microring resonator optical switches utilizing bias assisted carrier-injection induced refractive index change[J]. *Optics Express*, 2012, **20**(14): 15611-15627.

[8] LUO X S, SONG J F, FENG S Q, *et al*. Silicon high-order coupled-microring-based electro-optical switches for on-chip optical interconnects[J]. *IEEE Photonics Technology Letters*, 2012, **24**(10): 821-823.

[9] CHO S. Y., SOREF R. Interferometric microring-resonant 2×2 optical switches [J]. *Optics Express*, 2008, **16**(17): 13304-13314.

[10] YAN X, MA C S, ZHENG C T, *et al*. Analysis of polymer electro-optic microring resonator switches [J]. *Optics & Laser Technology*, 2010, **42**(3): 526-530.

[11] ZHENG C T, MA C S, YAN X, *et al*. Analysis of response characteristics for polymer directional coupler electro-optic switches [J]. *Optics Communications*, 2008, **281**(24): 5998-6005.

[12] ZHENG C T, MA C S, YAN X, *et al*. Design of integrated 1×2, 1×4 low driving voltage polymer electro-optic switches based onY-fed directional couplers[J]. *Journal of Modern Optics*, 2009, **56**(5): 615-622.

[13] ZHENG C T, MA C S, YAN X, *et al*. Optimal design and analysis of a high-speed, low-voltage polymer Mach-Zehnder interferometer electro-optic switch [J]. *Optics & Laser Technology*, 2010, **42**(3): 457-464.

[14] XU G Y, LIU Z F, MA J, *et al*. Organic electro-optic modulator using transparent conducting oxides as electrodes [J]. *Optics Express*, 2005, **13**(19): 7380-7385.

[15] PITOIS C, VUKMIROVIC S, HULT A, *et al*. Low-loss passive optical waveguides based on photo-sensitive poly (pentafluorostyrene-co-glycidyl methacrylate) [J]. *Macromolecules*, 1999, **32**(9): 2903-2909.

[16] DRISCOLL W G, VAUGHAN W. Handbook of Optics[M], New York: McGraw-Hill, 1978: 7.

[17] MA C S, LIU S Y. Optical Waveguide Mode Theory[M]. Changchun: Jilin University Press, 2006: Chapter 10.

[18] ZHENG C T, MA C S, CUI Z C, *et al*. Investigation on push-pull polymer Mach-Zehnder interferometer electro-optic switches using improved 3-D mode propagation analysis method[J]. *Optical and Quantum Electronics*, 2011, **42**(5): 327-346.